Video Article

Optocardiography and Electrophysiology Studies of Ex Vivo Langendorff-perfused Hearts

Luther M. Swift[1,2], Rafael Jaimes III[1,2], Damon McCullough[1,2], Morgan Burke[1,2], Marissa Reilly[1,2], Takuya Maeda[1,2,3], Hanyu Zhang[4], Nobuyuki Ishibashi[1,2,3], Jack M. Rogers[4], Nikki Gillum Posnack[1,2,5]

[1]Sheikh Zayed Institute for Pediatric Surgical Innovation, Children's National Hospital

[2]Children's National Heart Institute, Children's National Hospital

[3]Center for Neuroscience Research, Children's National Hospital

[4]Department of Biomedical Engineering, School of Engineering, University of Alabama at Birmingham

[5]Department of Pediatrics, Department of Pharmacology & Physiology, School of Medicine and Health Sciences, George Washington University

Correspondence to: Nikki Gillum Posnack at NPOSNACK@childrensnational.org

URL: https://www.jove.com/video/60472
DOI: doi:10.3791/60472

Keywords: Medicine, Issue 153, fluorescence, imaging, electrophysiology, heart, electrocardiogram, optical mapping, optocardiography

Date Published: 11/7/2019

Citation: Swift, L.M., Jaimes III, R., McCullough, D., Burke, M., Reilly, M., Maeda, T., Zhang, H., Ishibashi, N., Rogers, J.M., Posnack, N.G. Optocardiography and Electrophysiology Studies of Ex Vivo Langendorff-perfused Hearts. *J. Vis. Exp.* (153), e60472, doi:10.3791/60472 (2019).

Abstract

Small animal models are most commonly used in cardiovascular research due to the availability of genetically modified species and lower cost compared to larger animals. Yet, larger mammals are better suited for translational research questions related to normal cardiac physiology, pathophysiology, and preclinical testing of therapeutic agents. To overcome the technical barriers associated with employing a larger animal model in cardiac research, we describe an approach to measure physiological parameters in an isolated, Langendorff-perfused piglet heart. This approach combines two powerful experimental tools to evaluate the state of the heart: electrophysiology (EP) study and simultaneous optical mapping of transmembrane voltage and intracellular calcium using parameter sensitive dyes (RH237, Rhod2-AM). The described methodologies are well suited for translational studies investigating the cardiac conduction system, alterations in action potential morphology, calcium handling, excitation-contraction coupling and the incidence of cardiac alternans or arrhythmias.

Video Link

The video component of this article can be found at https://www.jove.com/video/60472/

Introduction

Cardiovascular disease is a leading cause of illness and death worldwide. As such, a primary research focus is to optimize methodologies that can be used to study normal cardiac physiology and underlying mechanisms that can contribute to morbidity and mortality in humans. Basic cardiovascular research has traditionally relied on small animal models, including rodents and rabbits[1,2,3], due to the availability of genetically modified species[4,5], lower-cost, smaller experimental footprint, and higher throughput. However, the use of a pig model has the potential to provide more clinically relevant data[6]. Indeed, previous studies have documented similarities in cardiac electrophysiology (EP) between humans and pigs, including similar ion currents[7], action potential shape[8], and responses to pharmacological testing[9]. Moreover, the porcine heart has contractile and relaxation kinetics that are more comparable to humans than either rodents or rabbits[10]. Compared to a canine model, the porcine coronary anatomy more closely resembles a human heart[11,12] and is the model of choice for studies focused on heart development, pediatric cardiology and/or congenital heart defects[13]. Although there are differences between the pig and human heart[8], these similarities make the porcine heart a valuable model for cardiovascular research[14].

Retrograde perfusion of the heart has become a standard protocol for studying cardiac dynamics ex vivo[15] since first established by Oskar Langendorff[16]. Accordingly, Langendorff-perfusion can be used to support an isolated, intact heart in the absence of autonomic influences. This model is a useful tool for directly comparing cardiac electrophysiology and contractility between healthy and non-healthy hearts. Since cardiac dynamics are both temporally and spatially complex, a slight alteration in one region can dramatically affect the entire heart's ability to work as a syncytium[17]. Therefore, high spatiotemporal imaging of parameter sensitive dyes is a useful tool for monitoring cardiac function across the surface of the heart[18,19]. Indeed, simultaneous dual imaging of voltage and calcium-sensitive fluorescent probes allows for the assessment of electrical activity, calcium handling and excitation-contraction coupling at the tissue level[20,21,22,23,24,25,26,27,28]. Langendorff-perfusion and/or optical mapping techniques have previously been used to document the decline in cardiac performance due to aging or genetic mutations, and to assess the safety of pharmacological agents or environmental exposures[29,30,31,32,33].

In the clinical setting, an invasive cardiac electrophysiology study is often used to investigate cardiac rhythm disturbances, identify pathologies, and pinpoint possible treatment options. Similarly, we describe an EP protocol that can be used to assess sinus node function, measure atrioventricular conduction, and identify the refractoriness of myocardial tissue. The described EP study can be performed in conjunction with

optical mapping, or optocardiography[34], to fully characterize cardiac physiology in isolated hearts. In the described protocol, high spatiotemporal resolution fluorescence imaging was performed with a combination of voltage (RH237) and calcium (Rhod-2AM) dyes in a dual emission setup. Additionally, cardiac electrophysiology parameters were monitored under both sinus rhythm and in response to programmed electrical stimulation.

Protocol

All experiments were conducted in accordance with the National Institutes of Health Guide for the Care and Use of Laboratory Animals (Eighth Edition). All methods and protocols used in these studies have been approved by the Institutional Animal Care and Use Protocol Committee at Children's National Hospital following the Guidelines for Care and Use of Laboratory Animals published by NIH. All animals used in this study received humane care in compliance with the Guide for the Care and Use of Laboratory Animals.

1. Preparation

1. Prepare 6 L of modified Krebs-Henseleit solution[16] (mM: 118.0 NaCl, 3.3 KCl, 1.2 $MgSO_4$, 24.0 $NaHCO_3$, 1.2 KH_2PO_4, 10.0 glucose, 2.0 sodium pyruvate, 2% albumin, 2.0 $CaCl_2$). Add $CaCl_2$ on the day of the experiment, since over time, in the presence of phosphates, calcium chloride will terminally precipitate out of solution as calcium phosphate.
2. Adjust the pH to 7.4 after sterile filtering (pore size: 0.22 µm). Check the solution osmolality to ensure a range of 275−310 mOsm/kg. Cool 1 L on ice for use immediately after the heart is excised. Warm 3 L in a water bath to approximately 37 °C before bubbling with carbogen (95% O_2, 5% CO_2).
   NOTE: Warming minimizes bubbles and potential embolism, since cold liquid has an increased capacity of gas to dissolve; therefore, as the modified Krebs-Henseleit media passes through the perfusion system and warms, the gas will be released as bubbles.
3. Prepare 2 L of cardioplegia (modified del Nido cardioplegia solution, **Table 1**). Freeze enough cardioplegia in an ice cube tray to fill a 500 mL beaker.
4. Turn on the circulating water baths set to 42 °C. Turn on the pumps to circulate the perfusate in a closed hydronic heating loop (for a full list of materials, see **Table of Materials** and **Figure 1**).
   NOTE: A heated circulating water bath is used to warm the water-jacketed tubes and heat exchangers.
5. Clean tubing circuits and chambers by running 2 L of a 1% solution of universal detergent in water through the system. Rinse all tubing circuits and chambers of the Langendorff system with >4 L of purified water. Run pumps until all water has been removed from the system.
6. Add a synthetic membrane filter in line with the perfusion pumps (polypropylene filter, pore size >5 µm). Gas a microfiber oxygenator (hemofilter) with 95% O_2 and 5% CO_2 at 80 kPa.
   NOTE: When using albumin, there is often frothing associated with oxygenation and/or the pumping activity through the tubing circuit. An anti-foam compound (antifoam Y30 emulsion) can be added dropwise periodically (~every 30 min) to quench it as it occurs.
7. Check a two-point calibration (0 and 60 mmHg) for the pressure sensor located above the aorta or in the bubble trap; calibrate as needed.
8. Immediately before heart excision, pour the media into the Langendorff loop perfusion system. Ensure that perfusate passes through microfiber oxygenators (hemofilters) gassed with oxygenated perfusate, which then flows through heat exchangers to maintain a media perfusate temperature of 37 °C at the aorta.
9. Set the circulating water bath to a few degrees higher than 37 °C, such as 42 °C, to account for heat loss during exchange and throughout the system. Monitor the circulating perfusate temperature with thermocouples.

2. Heart Excision and Langendorff-perfusion

1. Sedate the pig with an intramuscular (I.M.) injection of ketamine (20 mg/kg) and xylazine (2 mg/kg) and intubate with an endotracheal tube. For induction, administer an intravenous (I.V.) bolus injection of fentanyl (50 µg/kg) and rocuronium (1 mg/kg). Maintain anesthesia with inhaled Isoflurane (0.5−3%), fentanyl (10−25 µg/kg), and pancuronium (1 mg/kg).
   NOTE: For this proof-of-principle study, juvenile Yorkshire pigs (14−42 days old, n = 18) were used that ranged from 2.5−10.5 kg body weight and 18−137 g heart weight (**Figure 2**). If an additional injection for induction is necessary, ketamine (10 mg/kg) can be injected I.M.
2. **Once the animal is completely anesthetized and non-responsive, perform a sternotomy to expose the ascending aorta and right atrium.**
   1. Using a scalpel, make a midline incision from the top of the sternum at the thoracic inlet, down to the xiphoid process. With a cautery (or scissors), dissect the underlying fat and muscle until the sternum is visible.
   2. From the xiphoid process, cut the sternum midline up through the manubrium with either surgical bone scissors or a bone saw. Insert retractors into the incision to expose the heart.
3. Deliver a bolus dose of heparin (300 U/kg) to the right atria, using an 18 G needle and syringe, to minimize blot clots upon organ excision. Place absorbent pads in the chest cavity and ice around the heart.
4. With scissors, carefully slice through the pericardium, isolate the aorta by blunt dissection from the surrounding connective tissue, and clamp the aorta just below the first arterial branch on the aortic arch. Using a 50 mL syringe with an 18 G needle, inject ice-cold cardioplegia (20 mL/kg) through the top of the ascending aorta.
5. Cut through the vessels leading to the heart and remove the heart with the ascending aorta intact and plunge the excised heart into ice-cold cardioplegia.
6. Grasp the walls of the aorta with a pair of hemostats and slip it onto a ribbed cannula attached to tubing leading to 1 L of ice cold cardioplegia media suspended above the heart (~95 cm to provide ~70 mm Hg). Allow fluid to enter and fill the aorta until it overflows to prevent any bubble from entering the vasculature.
   NOTE: Use of a mechanical uncoupler (2,3-butanedione monoxime [BDM] or blebbistatin) will decrease the coronary perfusion rate as the oxygen demand of the tissue declines.
7. Secure the aorta to the cannula using umbilical tape and further anchor it by tying up the hemostats to bear the weight of the heart, which is now hanging from the cannula (**Figure 1C**). Allow the cold media to retrograde perfuse the heart at a constant pressure of 70 mmHg via

gravity. Keep the heart submerged in cold cardioplegia until ready to be transferred to the warmed (37 °C) Langendorff-perfusion system (<10 min).
NOTE: The aorta on smaller hearts (<50 g, up to 2 week-old pig) will bear the weight of the heart but larger hearts are at risk of slipping off the cannula. During the initial cannulation and when moving to the warmed system, prevent air from entering the aorta, which can cause coronary emboli. Use large bore tubing (>3/8" internal diameter) which allows bubbles to rise faster than the solution entering the aorta.

8. Transfer the heart to the Langendorff system (37 °C) without introducing air into the cannula. Allow the normal sinus rhythm to flush the vasculature of any remaining blood and cardioplegia.
NOTE: In the described study an average initial flow rate of 184 ± 17 mL/min was observed in isolated juvenile piglet hearts. The flow rate declined to 70 ± 7.5 mL/min (mean ± SEM) after perfusing with warmed media containing a mechanical uncoupler (20 mM BDM). Do not submerge the heart tissue, as it can impinge on cardiac imaging. Tissue temperature is maintained by coronary flow in the pig heart due to its larger volume and smaller surface area, as compared to rodents. Under full flow, the epicardium and endocardium temperatures ranged from 35 °C to 37 °C, respectively.
CAUTION: Wear appropriate personal protective equipment, including eye wear when working with mechanical uncouplers. The heart can eject media rapidly and unexpectedly.
9. Defibrillate the heart in the event of shockable arrhythmias (ventricular tachycardia, ventricular fibrillation) by placing external paddles at the apex and base of the heart and delivering a single shock at 5 J, increasing in 5 J increments (or as selectable by the defibrillator) until 50 J, cardioversion, or un-shockable rhythm. Repeat shocks at 50 J as necessary.
NOTE: In the presented study, 89% of preparations required defibrillation. After equilibration (~10 min), an average heart rate of 70 ± 4.5 bpm (mean ± SEM) was observed for juvenile piglet hearts (**Figure 2**).
10. Flush the heart with at least 1 L of modified Krebs-Henseleit media, without recirculating, to remove any residual blood and cardioplegia. Once the media runs clear through the heart, close the circulating loop to recirculate perfusate.

3. Electrophysiology Study

1. To record a standard lead II electrocardiogram (ECG) throughout the course of study, attach a 29 G needle electrode to the ventricular epicardium near the apex, with another electrode in the right atrium. Connect the positive and negative inputs of a differential bioamplifier to the apex and right atrium, respectively.
2. Attach one bipolar stimulus electrode on the right atria, and a second bipolar stimulus electrode to the lateral left ventricle for pacing purposes.
3. Pace the heart using an electrophysiology stimulator, with the initial current set to twice the diastolic threshold (1−2 mA) and a 1 ms pulse width[35,36].
NOTE: If the stimulation fails to elicit a response, the pulse width may be increased up to 2 ms. More current (~10x) is needed with large coaxial electrodes (bipolar stimulation).
4. Identify the pacing threshold by applying a series of stimulus impulses (1−2 mA, 1 ms pulse width) at defined pacing cycle lengths (PCL) to ensure consistent stimulus response.
NOTE: Once the intrinsic rate is established, the initial impulse train may begin at a slightly shorter PCL.
5. **Perform extrastimulus pacing using either an S1−S1 or S1−S2 pacing train, in the latter a train of 6−8 impulses (S1) was followed by a single impulse (S2). Decrease the S2 PCL stepwise by 10 ms (i.e., 200 ms, 190 ms, 180 ms, etc.) until it fails to capture. Step up to the penultimate PCL (i.e., 190 ms) and decrease in 1 ms intervals to find the most precise PCL before the loss of capture (i.e., 184 ms).**
NOTE: The same stimulation parameters are used for both S1 and S2 (1−2 mA, 1 ms pulse width). See **Figure 3** for representative examples, or previously published values on porcine heart electrophysiology measurements[37].
    1. To establish the ventricular effective refractory period (VERP), use the stimulus electrode on the lateral left ventricle to identify the shortest S1−S2 interval at which the S2 (premature beat) initiates ventricular depolarization.
    NOTE: The refractory period is the shortest achievable S1−S2 coupling interval.
    2. To define the Wenckebach cycle length (WBCL), use the stimulus electrode on the right atrium to find the shortest S1−S1 interval at which 1:1 atrioventricular conduction propagates via the normal conduction pathway.
    NOTE: Failure to do so represents 2nd degree heart block.
    3. To define the sinus node recovery time (SNRT), use the stimulus electrode on the right atrium to apply a pacing train (S1−S1) and measure the time delay between the last impulse in the pacing train, and the recovery of spontaneous sinoatrial node-mediated activity.
    4. To establish atrioventricular node effective refractory period (AVNERP), use the stimulus electrode on the right atrium to find the shortest S1−S2 coupling interval at which the premature atrial stimulation is followed by a His bundle potential that elicits a QRS complex, which signifies ventricular depolarization.

4. Optical Mapping of Transmembrane Voltage and Intracellular Calcium

NOTE: A mechanical uncoupler should be used to minimize motion artifacts during optical mapping and to avoid hypoxia[3,38,39,40]. (-/-)Blebbistatin (5 µM circulating concentration) may be added slowly as a bolus dose of 0.5 mM in 5 mL of perfusate (100x of final concentration)[41]. Alternatively, BDM may be initially included in the perfusate media at a circulating concentration of 20 mM.

1. Prepare the voltage dye by dissolving 5 mg of RH237 into 4 mL of anhydrous DMSO. Dilute the dye aliquot with up to 5 mL of media and vortex. Slowly add RH237 (62.1 µg per 500 mL of perfusate) proximal to the aortic cannula.
NOTE: The myocardial tissue may be re-stained with RH237, if needed, throughout the duration of the experiment.
2. Prepare the calcium dye by dissolving 1 mg of Rhod2-AM into 1 mL of anhydrous DMSO. Mix the dye with 50 µL of pluronic acid, place in a 37 °C sonicating bath for up to 10 min, and then dilute with up to 5 mL of media. Slowly add the calcium dye (50 µg per 500 mL of perfusate) proximal to the aortic cannula.
NOTE: To ensure uniform dye staining, dyes should be added slowly (>30 s). Rhod-2AM takes up to 10 min to reach peak fluorescence, while RH237 stains the heart within a 1−2 min. Using the described dye loading, signal to noise ratio (SNR) ranges of ~42−86 and ~35−69

for voltage and calcium, respectively, can be expected. SNR values can be calculated as SNR = (Peak-to-Peak counts)/(Standard deviation during diastolic interval)[42].

3. Position the imaging hardware (camera, image splitter, lens) as shown in **Figure 1**, to focus on an appropriate field of view.
   NOTE: The splitter is configured with a dichroic mirror (660+ nm) that passes RH237 and reflects Rhod2 emission spectra. High-transmission emission filters are used for the RH237 (710 nm long pass) and Rhod2 (585 ± 40 nm) emitted light (long pass ET710, see **Table of Materials**). A wide-pupil 50 mm/F0.95l lens is attached to the front of the image splitter. This configuration results in adequate emission light separation, as previously validated[43,44].
4. Connect the camera to a workstation and acquire images using selected software, with an exposure time of 0.5−2 ms. Perform image alignment with the aid of software that can split the desired regions, overlay, and display a gray-scale subtraction or pseudo-color addition to highlight misalignment (see **Table of Materials** for software option).
5. Turn off the room light to minimize fluorescence interference from ambient lighting. Test the LED lights (525 nm, 1.4 mW/mm^2) prior to the start of imaging to ensure uniform and maximal epicardial illumination, as determined by the sensor well depth.
   NOTE: Each light is directed through an excitation filter (535 ± 25 nm). LED lights can be triggered manually before filming to maximize signal linearity. Emitted fluorescence from the epicardium is passed through the image splitter and emission filters. Split images are projected onto a high-speed sensor. The field of view of is approximately 12 cm x 10 cm, or 5.9 cm x 4.7 cm for each split image, depending on lens choice and distance from the heart.
6. For optical mapping studies, image the myocardium during sinus rhythm, ventricular fibrillation (**Figure 4**) or dynamic pacing (S1−S1, 1−2 mA, 1 ms pulse width) via a stimulation electrode positioned on the left ventricle (**Figure 5**). Begin with a pacing cycle length of 350 ms, and decrement by 10−50 ms to generate restitution curves (**Figure 5E**)[35,36].

5. Cleanup

1. Remove the heart from the system and drain all perfusate. Rinse the system tubing and chambers with purified water.
2. For routine maintenance, periodically rinse the system with detergent solution or a diluted hydrogen peroxide solution, as needed.

6. Data Processing

1. Confirm optical signal quality throughout the study by opening a video file, selecting a region of interest, and plotting mean fluorescence over time using an appropriate software package or custom algorithm.
2. **Analyze imaging data as previously described[23,33,43,45,46], to quantify action potential and calcium transient temporal parameters, including activation time, voltage-calcium coupling time (difference between Vm and Ca activation times), and repolarization duration measurements.**
   1. Apply thresholding to isolate fluorescent epicardial pixels and discard noisy background data.
      NOTE: Thresholding will simplify and speed up analysis across large videos.
   2. Spatially filter optical signals over an epicardial surface area with kernel sizes ranging from 3 mm x 3 mm to 5 mm x 5 mm, as seen in **Figure 4** and **Figure 5**.
      NOTE: The latter will improve the SNR without distorting action potential features, calcium transient morphology, or overall contour of the wavefronts[19,47]. This may be unnecessary if using a sensor with large pixels or if binning during acquisition.
   3. Temporally filter signals with a digital lowpass filter (e.g., 5th-order Butterworth) with a cutoff frequency between 100 and 75 Hz to eliminate insignificant signal content[45].
      NOTE: See **Figure 5C** for an example of representative processed traces.
   4. Apply drift removal and subtraction, via Nth-order polynomial fitting, to minimize the effects of photobleaching, motion, or other significant sources of variation.
   5. After processing and normalization of optical data across an entire video, calculate action potential and calcium transient parameters of interest. Determine activation time, defined as the time of maximum derivative during depolarization, and peak fluorescence in order to calculate repolarization percentage times and periods (action potential duration [APD] and [Ca^{2+}]i duration [CaD], see **Figure 5**).
   6. After temporal parameters are calculated, generate isochronal maps to depict aspects of a single action potential or calcium transient across the entire imaged epicardial surface using custom algorithms[23,33,43,45,46].
      NOTE: See **Figure 5D** for an example.

Representative Results

Figure 1A shows a diagram of the isolated heart perfusion system, which includes the tubing circuit, pump, filter, oxygenator, reservoirs and heating elements. Placement of the ECG (lead II configuration) and pacing electrodes is shown in **Figure 1B**, and the imaging setup is depicted in **Figure 1C**. A schematic of the optical components and light paths are shown in **Figure 1D**.

Experimental studies were performed on intact, whole hearts isolated from juvenile Yorkshire pigs (14−42 days, n = 18) that ranged in size from 2.5−10.5 kg body weight and 18−137 g heart weight (**Figure 2A**). After transferring the isolated heart to a Langendorff system (37 °C), the heart rate stabilized to 70 ± 4.5 bpm (mean ± SEM) within ~10 min of defibrillation and remained constant throughout the duration of study (**Figure 2B**). An average flow rate of 184 ± 17 mL/min (mean ± SEM) was measured, which slowed to 70 ± 7.5 mL/min after perfusing with warmed media containing a mechanical uncoupler (**Figure 2C**).

Lead II ECGs were recorded throughout the duration of the study during sinus rhythm (**Figure 3A**) or in response to external pacing (**Figure 3B-E**) to quantify electrophysiological parameters**.** For EP assessment, dynamic pacing (S1−S1) was applied to the right atrium to pinpoint the WBCL and SNRT (recovery time after S1−S1 commences, **Figure 3C**), wherein WBCL was denoted as the shortest PCL that initiated atrial to ventricular conduction. An S1−S2 pacing protocol was implemented using a bipolar stimulus electrode on the left ventricle in order to identify the shortest coupling interval that initiated ventricular depolarization, thereby pinpointing VERP (**Figure 3D**). Alternatively, an S1−S2 atrial pacing

protocol is applied to pinpoint AVNERP (S1−S2), as shown in **Figure 3E**. Representative examples of pig heart electrophysiology parameters align closely with those previously published[37].

Optical mapping experiments were performed during sinus rhythm, spontaneous ventricular fibrillation (**Figure 4**), or during dynamic pacing (S1−S1) of the left ventricle (LV) to generate electrical and calcium restitution curves depicted in **Figure 5**. Representative images of a dye-loaded piglet heart are shown in **Figure 4** with corresponding optical action potentials (Vm) and calcium (Ca) transients collected from two regions of interest on the epicardial surface (right ventricle [RV] = blue, LV = red). Unprocessed signals are displayed during sinus rhythm and during ventricular fibrillation. As previously mentioned, dynamic epicardial pacing (S1−S1) was also used during optical mapping experiments to normalize any slight difference in the intrinsic heart rate (**Figure 5A-E**). Raw signals are displayed (RV = blue, LV = red), which were used to depict the action potential — calcium transient coupling time (**Figure 5C**), activation and duration time (**Figure 5D**), electrical and calcium restitution (**Figure 5E**). For thick myocardial preparations, spatial filtering with kernel size ~3 mm x 3 mm is appropriate for epicardial action potential or calcium transient analysis[19,47]. Accordingly, high spatial resolution images (in the described setup 1240 x 1024 total, or 620 x 512 per channel, 6.5 µm pixel size) are often spatially binned during or post-acquisition (**Figure 5C**). Image processing can be performed to generate activation and repolarization maps using custom algorithms[23,33,43,45] (**Figure 3D**), with the activation time of each pixel on the heart was defined as the maximum derivative of the action potential or calcium transient upstroke.

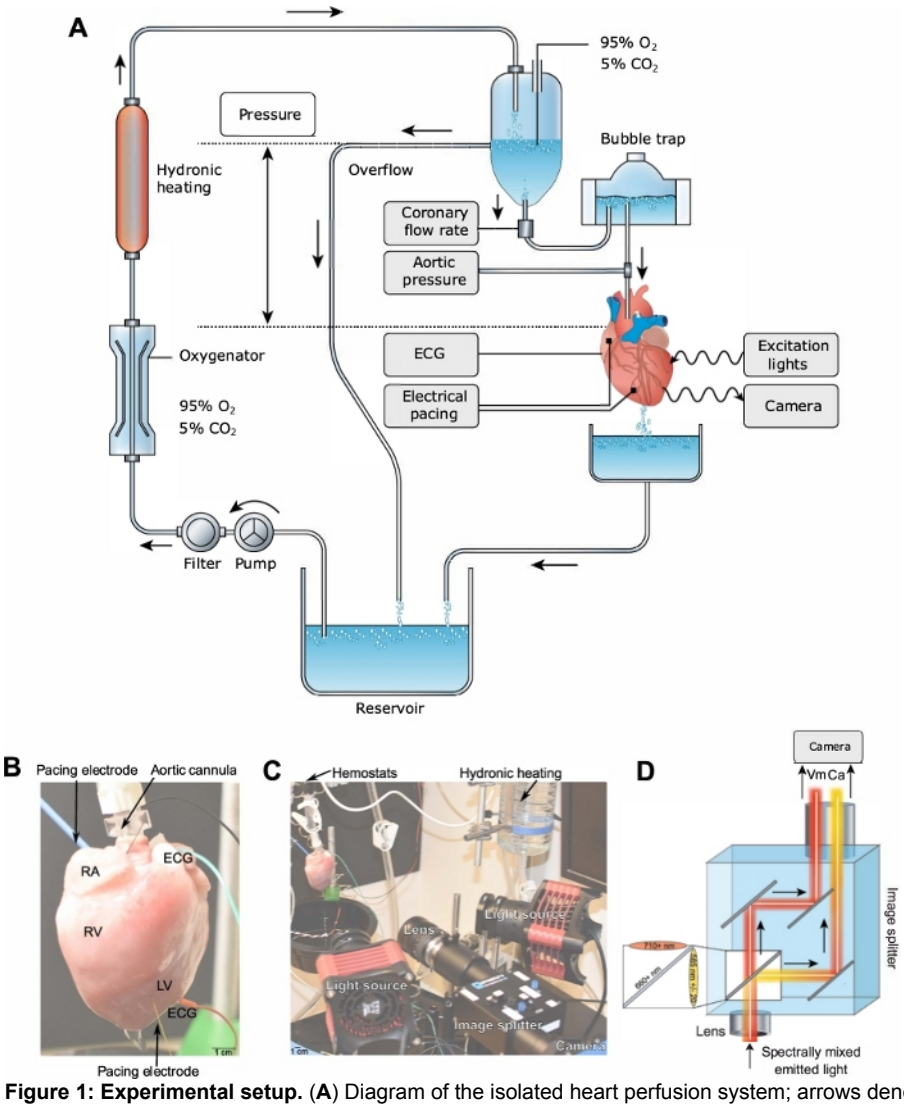

Figure 1: Experimental setup. (**A**) Diagram of the isolated heart perfusion system; arrows denote the direction of flow. (**B**) A cannulated heart is shown with electrode placement. RA = right atria, RV = right ventricle, LV = left ventricle, ECG = lead II electrocardiogram. (**C**) The imaging platform in close proximity to the heart tissue. (**D**) Emission of each complementary probe (voltage, calcium) is separated by wavelength using an image splitting device with appropriate emission filters and dichroic mirror. Please click here to view a larger version of this figure.

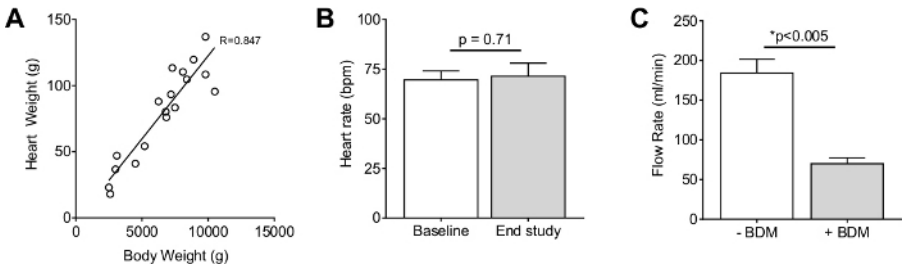

Figure 2: Heart weight, rate and flow measurements. (**A**) Heart weight to body weight ratio for each piglet used in the study (n = 18). (**B**) Heart rate measured ~10 min after defibrillation and again at the end of study (approximately 1 h). (**C**) Coronary flow drops precipitously after perfusion with a mechanical uncoupler (+BDM) due to reduced oxygen demand. Scale bars represent mean ± SEM. Please click here to view a larger version of this figure.

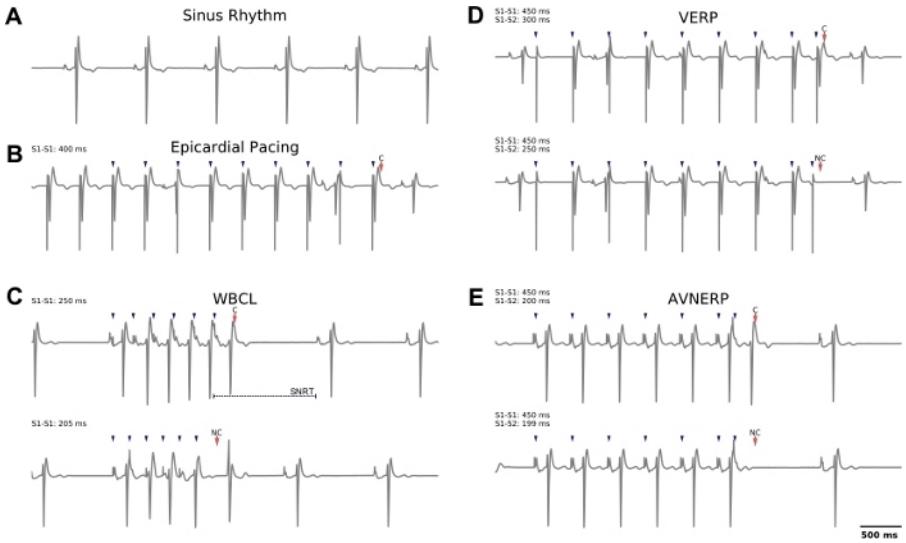

Figure 3: Representative examples of lead II electrocardiogram recordings collected during sinus rhythm or in response to external pacing. (**A**) Normal sinus rhythm. (**B**) Example of epicardial pacing at cycle length of 400 ms (S1−S1), which was used for imaging experiments. (**C**) Top: Atrial pacing to identify WBCL; successful capture is observed at S1 = 250 ms wherein atrial to ventricular conduction is observed. Note that atrial pacing can be used to determine SNRT (time to sinus node discharge, after commencing external pacing). Bottom: As the S1 cycle length is decreased to 205 ms, the conduction to the ventricle fails. (**D**) Top: Epicardial pacing (S1−S2) to identify VERP; successful capture is observed at S1 = 450 ms, S2 = 300 ms. Bottom: As the S2 cycle length is decreased to 250 ms, the ventricular tissue fails to capture. (**E**) Atrial pacing (S1−S2) to identify AVNERP. Top: Successful capture is observed at S1 = 450 ms, S2 = 200 ms. Bottom: As the S2 cycle length is decreased to 199 ms, conduction to the ventricle fails. Blue arrows denote pacing spikes, red arrows denote capture ('C') or no capture ('NC'). S1−S1 = dynamic pacing, S1−S2 = extrastimulus pacing. Please click here to view a larger version of this figure.

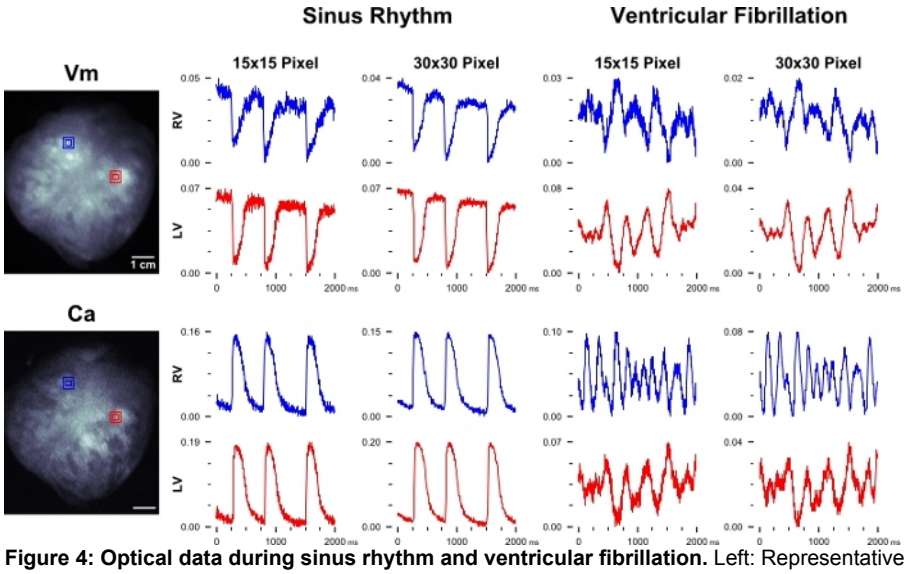

Figure 4: Optical data during sinus rhythm and ventricular fibrillation. Left: Representative images of a dye-loaded pig heart (Vm = voltage, RH237; Ca = calcium, Rhod2), anterior view. Spatially filtered transmembrane voltage and intracellular calcium fluorescent signals from a pig heart during sinus rhythm (Center). Voltage and calcium signals during ventricular fibrillation (Right). Signal region sizes (15 x 15 pixels = 2.4 x 2.4 mm^2, 30 x 30 = 4.8 x 4.8 mm^2 kernel size) represented as red and blue squares. Units = ΔF/F. Please click here to view a larger version of this figure.

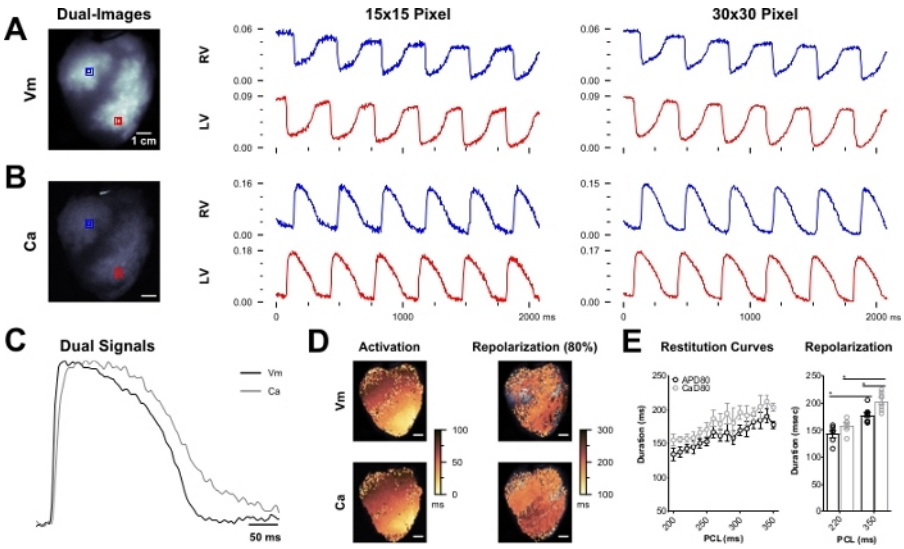

Figure 5: Optical data from Langendorff-perfused pig hearts. Unprocessed, spatially filtered (**A**) transmembrane voltage and (**B**) intracellular calcium fluorescence signals from the right and left ventricles during electrical pacing at the apex. Unfiltered, spatially averaged signals depict optical action potentials and calcium transients from regions of interest (signal units are ΔF/F). (**C**) An overlay of normalized transients illustrates action potential-calcium transient coupling time (low-pass filtered at 75 Hz). (**D**) Processing signals across the epicardial surface to generate isochronal maps of temporal parameters, including activation time (t_{act}) and 80% repolarization time. (**E**) Electrical and calcium transient restitution curves generated at multiple frequencies (left) with statistical analysis (right) to illustrate longer repolarization time at slower pacing cycle lengths. Scale bars = mean ± SEM. Please click here to view a larger version of this figure.

Chemical	Formula	Molecular weight	g/L
Sodium chloride	NaCl	58.44	5.26
Sodium gluconate	$C_6H_{11}NaO_7$	218.14	5.02
Sodium acetate trihydrate	$C_2H_3NaO_2 \cdot 3H_2O$	136.08	3.68
Potassium chloride	KCl	74.55	0.63
Magnesium chloride (anhydrous)	$MgCl_2$	95.21	0.1405
8.4% Sodium bicarbonate	$NaHCO_3$	84.01	13
Mannitol	$C_6H_{14}O_6$	182.17	16.3
Magnesium sulfate	$MgSO_4$	120.37	4
pH	7.4		
Osmolarity (mOsmol/L)	294		

Table 1: Modified del Nido's cardioplegia recipe.

Discussion

Although cardiovascular research models range from cellular to in vivo preparations, there is an inherent trade-off between clinical relevance and experimental utility. On this spectrum, the isolated Langendorff-perfused heart remains a useful compromise for studying cardiac physiology[48]. The whole heart model represents a higher level of functional and structural integration than single cell or tissue monolayers, but also avoids the confounding complexities associated with in vivo models. A major advantage during dual optical mapping experiments is that the epicardial surface of the isolated heart can be observed, and fluorescence imaging of transmembrane potential and calcium handling can be used to monitor cardiac physiology[34].

Rodent models are most commonly used for isolated heart preparations as opposed to larger animals, due in part to the associated cost of up-sizing all the elements involved (e.g., solution volume, perfusion circuit, quantity of dyes and mechanical uncouplers) along with greater instability and propensity for arrhythmias in larger animals[10,36,49]. One advantage to using pig hearts is that they closely resemble the human heart in structure, size and rate of contraction, therefore more accurately modeling hemodynamic parameters like coronary blood flow and cardiac output. Likewise, humans and pigs have similar calcium handling, electrocardiogram intervals[37], and action potential morphology including the underlying channels that it represents[12,50,51,52]. This protocol describes in detail the steps for creating a reproducible large animal model to comprehensively characterize myocardial function. Simultaneous imaging of transmembrane voltage (RH237) and intracellular calcium (Rhod2), used in conjunction with established electrophysiological protocols, provides the opportunity to pinpoint mechanisms that are responsible for altered cardiac function. The described methodology can be used for preclinical safety testing, toxicological screening and the investigation of genetic or other disease pathologies. Moreover, the described methodology can be modified and adapted for use with other cardiac models (e.g., canine, human) depending on the specific research focus[53,54,55].

There are a few critical modifications to keep in mind when transitioning from a smaller rodent model to a larger pig model for isolated, whole heart preparations. During preparation and setup, we recommend adding albumin to the perfusate to maintain oncotic pressure and reduce edema (plus antifoam, if needed)[56,57,58,59]. Moreover, perfusate containing albumin can also aid in metabolic studies that also require fatty acid-supplementation to the media[60,61]. Unlike rodent hearts, the larger pig heart does not need to be submerged in warm media due to its smaller surface to volume ratio and the increased volume of warmed media flowing through the coronary vessels which better maintains the temperature. As noted earlier, we placed temperature probes inside the right ventricle and on the epicardial surface of both the right and left ventricles, observing only slight temperature fluctuations of 1−2 °C in all three locations throughout the study. Importantly, such faster flow rates can also increase the likelihood of bubbles and a potential embolism. To circumvent this problem, we recommend using a bubble trap with large bore tubing leading straight down to the aortic cannula. Similarly, we found it most useful to have two individuals working in tandem to cannulate the aorta on a larger (and heavier) heart; one person to hold the aorta open with sturdy hemostats and another to secure the aorta to the canula using umbilical tape. In the described methodology, we found that perfusion with cardioplegia and defibrillation were vital to cardiac recovery, which is contrary to rodent heart preparations. In our experience, only a few excised hearts resumed normal sinus-driven activity without cardioversion.

To improve optical imaging endpoints, a hanging heart preparation limited the effect of glare that can occur with a submerged heart. Moreover, the hanging heart also avoids any compression or compromise of the coronary vessels on the posterior aspect of the heart that can occur when laying the heart down horizontally for vertical imaging. We also found that loading fluorescent dyes after the bubble trap (close to the aortic cannula) greatly improved tissue staining and optical signals. Finally, to improve cardiac electrophysiology endpoints, the use of a larger coaxial stimulation electrode facilitated successful atrial pacing. Although we describe the use of electrocardiograms to identify capture and loss of capture for various EP parameters, intracardiac catheters or bipolar recording electrodes can also be used.

Our study was focused on developing a methodology for dual optical mapping and cardiac electrophysiological assessment in an isolated, intact porcine heart model. Due to similarities with the juvenile human heart, the porcine heart remains a popular model for studies focused on pediatric cardiology or congenital heart defects. Importantly, the described approach can be adapted to use with larger sized adult hearts and/or different species of interest. Indeed, other laboratories may find that the use of canine or human hearts (either donor or diseased) are more applicable for their specific research focus[53,54,55]. Another potential limitation to this study is the use of a mechanical uncoupler to reduce motion artifact during imaging. Blebbistatin has become the uncoupler of choice in cardiac imaging applications due to its minimal effects on ECG parameters, activation and refractory periods[41,62,63]. BDM is a less expensive choice, which can be particularly important in large animal studies

that require greater volumes of perfusate and mechanical uncoupler, but it is known to have a greater impact on potassium and calcium currents that can alter action potential morphology[64,65,66,67]. If BDM is used, note that APD shortening increases the hearts vulnerability to shock-induced arrythmias[68]. Conversely, the main limitation to using blebbistatin is its photosensitivity and phototoxicity, although alternative formulations that have reduced these effects[69,70,71]. Finally, the described methodology utilizes a single camera system for dual optical mapping experimentation, but it is important to note that research studies focused on ventricular fibrillation and/or tracking of electrical waves across the epicardial surface would need to modify this approach to include three-dimensional panoramic imaging, as described by others[15,19,72,73,74,75].

Disclosures

The authors have nothing to disclose.

Acknowledgments

The authors gratefully acknowledge Dr. Matthew Kay for helpful experimental guidance, and Manelle Ramadan and Muhaymin Chowdhury for technical assistance. This work was supported by the National Institutes of Health (R01HL139472 to NGP, R01 HL139712 to NI), Children's Research Institute, Children's National Heart Institute and Sheikh Zayed Institute for Pediatric Surgical Innovation.

References

1. Wang, L., De Jesus, N.M., Ripplinger, C.M. Optical Mapping of Intra-Sarcoplasmic Reticulum Ca2+ and Transmembrane Potential in the Langendorff-perfused Rabbit Heart. *Journal of Visualized Experiments.* (103), e53166 (2015).
2. Lang, D., Sulkin, M., Lou, Q., Efimov, I.R. Optical Mapping of Action Potentials and Calcium Transients in the Mouse Heart. *Journal of Visualized Experiments.* (55), e3275 (2012).
3. Asfour, H., Wengrowski, A.M., Jaimes III, R., Swift, L.M., Kay, M.W. NADH fluorescence imaging of isolated biventricular working rabbit hearts. *Journal of Visualized Experiments.* (65), e4115 (2012).
4. Capecchi, M.R. The new mouse genetics: altering the genome by gene targeting. *Trends in genetic.* **5** (3), 70–6 (1989).
5. Hall, B., Limaye, A., Kulkarni, A.B. Overview: generation of gene knockout mice. *Current Protocols in Cell Biology.* **Chapter 19**, Unit 19.12 19.12.1-17 (2009).
6. Schechter, M.A. *et al.* An Isolated Working Heart System for Large Animal Models. *Journal of Visualized Experiments.* (88), e51671 (2014).
7. Arlock, P. et al. Ion currents of cardiomyocytes in different regions of the Göttingen minipig heart. *Journal of Pharmacological and Toxicological Methods.* **86**, 12–18 (2017).
8. Crick, S.J., Sheppard, M.N., Ho, S.Y., Gebstein, L., Anderson, R.H. Anatomy of the pig heart: comparisons with normal human cardiac structure. *Journal of anatomy.* **193** (Pt 1) 105–19 (1998).
9. Markert, M. et al. Validation of the normal, freely moving Göttingen minipig for pharmacological safety testing. *Journal of Pharmacological and Toxicological Methods.* **60** (1), 79–87 (2009).
10. Milani-Nejad, N., Janssen, P.M.L.M.L. Small and large animal models in cardiac contraction research: advantages and disadvantages. *Pharmacology & Therapeutics.* **141** (3), 235–49 (2014).
11. Bertho, E., Gagnon, G. A comparative study in three dimension of the blood supply of the normal interventricular septum in human, canine, bovine, porcine, ovine and equine heart. *Diseases of the Chest.* **46**, 251–62 (1964).
12. Lelovas, P.P., Kostomitsopoulos, N.G., Xanthos, T.T. A comparative anatomic and physiologic overview of the porcine heart. *Journal of the American Association for Laboratory Animal Science.* **53** (5), 432–8 (2014).
13. Camacho, P., Fan, H., Liu, Z., He, J.Q. Large Mammalian Animal Models of Heart Disease. *Journal of Cardiovascular Development and Disease.* **3** (4), 30 (2016).
14. Jordan, C.P. *et al.* Minimally Invasive Resynchronization Pacemaker: A Pediatric Animal Model. *The Annals of Thoracic Surgery.* **96** (6), 2210–2213 (2013).
15. Rogers, J.M., Walcott, G.P., Gladden, J.D., Melnick, S.B., Kay, M.W. Panoramic optical mapping reveals continuous epicardial reentry during ventricular fibrillation in the isolated swine heart. *Biophysical Journal.* **92** (3), 1090–1095 (2007).
16. Langendorff, O. Untersuchungen am uberlebenden Saugethierherzen [Investigations on the surviving mammalian heart]. *Pflügers Archiv: European Journal of Physiology.* **61**, 291–332 (1895).
17. Pumir, A., Arutunyan, A., Krinsky, V., Sarvazyan, N. Genesis of ectopic waves: role of coupling, automaticity, and heterogeneity. *Biophysical Journal.* **89** (4), 2332–2349 (2005).
18. Kay, M.W., Walcott, G.P., Gladden, J.D., Melnick, S.B., Rogers, J.M. Lifetimes of epicardial rotors in panoramic optical maps of fibrillating swine ventricles. *American journal of Physiology - Heart and Circulatory Physiology.* **291** (4), H1935-41 (2006).
19. Lee, P. *et al.* Low-Cost Optical Mapping Systems for Panoramic Imaging of Complex Arrhythmias and Drug-Action in Translational Heart Models. *Scientific Reports.* **7**, 43217 (2017).
20. Venkataraman, R., Holcomb, M.R., Harder, R., Knollmann, B.C., Baudenbacher, F. Ratiometric imaging of calcium during ischemia-reperfusion injury in isolated mouse hearts using Fura-2. *BioMedical Engineering OnLine.* **11** (1), 39 (2012).
21. Efimov, I.R., Nikolski, V.P., Salama, G. Optical Imaging of the Heart. *Circulation Research.* **95** (1), 21–33 (2004).
22. Zimmermann, W.H. et al. Three-dimensional engineered heart tissue from neonatal rat cardiac myocytes. *Biotechnology and Bioengineering.* **68** (1), 106–114 (2000).
23. Jaimes, R. et al. A Technical Review of Optical Mapping of Intracellular Calcium within Myocardial Tissue. *American Journal of Physiology-Heart and Circulatory Physiology.* **310** (11), H1388–401 (2016).
24. Herron, T.J., Lee, P., Jalife, J. Optical imaging of voltage and calcium in cardiac cells & tissues. *Circulation Research.* **110** (4), 609–623 (2012).
25. Guatimosim, S., Guatimosim, C., Song, L.S. Imaging Calcium Sparks in Cardiac Myocytes. *Methods in Molecular Biology (Clifton, N.J.).* **689**, 205 (2011).

26. Hou, J.H., Kralj, J.M., Douglass, A.D., Engert, F., Cohen, A.E. Simultaneous mapping of membrane voltage and calcium in zebrafish heart in vivo reveals chamber-specific developmental transitions in ionic currents. *Frontiers in Physiology.* **5**, 344 (2014).
27. Thomas, K., Goudy, J., Henley, T., Bressan, M. Optical Electrophysiology in the Developing Heart. *Journal of Cardiovascular Development and Disease.* **5** (2), 28 (2018).
28. Nikolski, V., Efimov, I. Fluorescent imaging of a dual-pathway atrioventricular-nodal conduction system. *Circulation Research.* **88** (3), E23-30 (2001).
29. Posnack, N.G. et al. Bisphenol A Exposure and Cardiac Electrical Conduction in Excised Rat Hearts. *Environmental Health Perspectives.* **122** (4), 384–90 (2014).
30. Garrott, K. et al. KATP channel inhibition blunts electromechanical decline during hypoxia in left ventricular working rabbit hearts. *The Journal of Physiology.* **595** (12), 3799–3813 (2017).
31. Wang, Z. et al. Exposure to Secondhand Smoke and Arrhythmogenic Cardiac Alternans in a Mouse Model. *Environmental Health Perspectives.* **126** (12), 127001 (2018).
32. Francis Stuart, S.D. et al. Age-related changes in cardiac electrophysiology and calcium handling in response to sympathetic nerve stimulation. *The Journal of Physiology.* **596** (17), 3977–3991 (2018).
33. Jaimes, R. et al. Plasticizer Interaction With the Heart: Chemicals Used in Plastic Medical Devices Can Interfere With Cardiac Electrophysiology. *Circulation: Arrhythmia and Electrophysiology.* **12** (7), (2019).
34. Boukens, B.J., Efimov, I.R. A century of optocardiography. *IEEE reviews in Biomedical Engineering.* **7**, 115–125 (2014).
35. Li, N., Wehrens, X.H. Programmed Electrical Stimulation in Mice. *Journal of Visualized Experiments.* (39), e1730 (2010).
36. Dor-Haim, H., Berenfeld, O., Horowitz, M., Lotan, C., Swissa, M. Reduced Ventricular Arrhythmogeneity and Increased Electrical Complexity in Normal Exercised Rats. *PLoS ONE.* **8** (6), e66658 (2013).
37. Noszczyk-Nowak, A. *et al.* Normal Values for Heart Electrophysiology Parameters of Healthy Swine Determined on Electrophysiology Study. *Advances in Clinical and Experimental Medicine.* **25** (6), 1249–1254 (2016).
38. Wengrowski, A.M., Kuzmiak-Glancy, S., Jaimes, R., Kay, M.W. NADH changes during hypoxia, ischemia, and increased work differ between isolated heart preparations. *American Journal of Physiology-Heart and Circulatory Physiology.* **306** (4), H529-37 (2014).
39. Schramm, M., Klieber, H.G., Daut, J. The energy expenditure of actomyosin-ATPase, Ca(2+)-ATPase and Na+,K(+)-ATPase in guinea-pig cardiac ventricular muscle. *The Journal of Physiology.* **481** (Pt 3), 647–62 (1994).
40. Kuzmiak-Glancy, S. et al. Cardiac performance is limited by oxygen delivery to the mitochondria in the crystalloid-perfused working heart. *American Journal of Physiology- Heart and Circulatory Physiology.* **314** (4), H704–H715 (2018).
41. Fedorov, V. V et al. Application of blebbistatin as an excitation-contraction uncoupler for electrophysiologic study of rat and rabbit hearts. *Heart Rhythm.* **4**, (5), 619–626 (2007).
42. Evertson, D.W. et al. High-Resolution High-Speed Panoramic Cardiac Imaging System. *IEEE Transactions on Biomedical Engineering.* **55** (3), 1241–1243 (2008).
43. Jaimes, R. *et al.* Lights, Camera, Path Splitter: A New Approach for Truly Simultaneous Dual Optical Mapping of the Heart with a Single Camera. *bioRxiv.* 651380 (2019).
44. Choi, B.R., Salama, G. Simultaneous maps of optical action potentials and calcium transients in guinea-pig hearts: mechanisms underlying concordant alternans. *Journal of Physiology.* **529** 171–188 (2000).
45. Laughner, J.I., Ng, F.S., Sulkin, M.S., Arthur, R.M., Efimov, I.R. Processing and analysis of cardiac optical mapping data obtained with potentiometric dyes. *American Journal of Physiology-Heart and Circulatory Physiology.* **303** (7), H753-65 (2012).
46. O'Shea, C. et al. ElectroMap: High-throughput open-source software for analysis and mapping of cardiac electrophysiology. *Scientific Reports.* **9** (1), 1389 (2019).
47. Mironov, S.F., Vetter, F.J., Pertsov, A.M. Fluorescence imaging of cardiac propagation: spectral properties and filtering of optical action potentials. *American Journal of Physiology-Heart and Circulatory Physiology.* **291** (1), H327-335 (2006).
48. Skrzypiec-Spring, M., Grotthus, B., Szelag, A., Schulz, R. Isolated heart perfusion according to Langendorff---still viable in the new millennium. *Journal of Pharmacological and Toxicological Methods.* **55** (2), 113–126 (2007).
49. Nishida, K., Michael, G., Dobrev, D., Nattel, S. Animal models for atrial fibrillation: clinical insights and scientific opportunities. *Europace.* **12** (2), 160–172 (2010).
50. Verdouw, P.D., Van Den Doel, M.A., De Zeeuw, S., Duncker, D.J. Animal models in the study of myocardial ischaemia and ischaemic syndromes. *Cardiovascular Research.* **39** (1), 121-135 (1998).
51. Camacho, P., Fan, H., Liu, Z., He, J.Q. Large Mammalian Animal Models of Heart Disease. *Journal of Cardiovascular Development and Disease.* **3** (4), 30 (2016).
52. Swindle, M.M., Makin, A., Herron, A.J., Clubb, F.J., Frazier, K.S. Swine as Models in Biomedical Research and Toxicology Testing. *Veterinary Pathology.* **49** (2), 344–356 (2012).
53. Aras, K.K., Faye, N.R., Cathey, B., Efimov, I.R. Critical Volume of Human Myocardium Necessary to Maintain Ventricular Fibrillation. *Circulation: Arrhythmia and Electrophysiology.* **11** (11), e006692 (2018).
54. Hill, A.J. *et al.* In Vitro Studies of Human Hearts. *The Annals of Thoracic Surgery.* **79** (1), 168–177 (2005).
55. Fedorov, V. V *et al.* Structural and functional evidence for discrete exit pathways that connect the canine sinoatrial node and atria. *Circulation Research.* **104** (7), 915–923 (2009).
56. Jacob, M. *et al.* Albumin Augmentation Improves Condition of Guinea Pig Hearts After 4 hr of Cold Ischemia. *Transplantation.* **87** (7), 956–965 (2009).
57. Segel, L.D., Ensunsa, J.L. Albumin improves stability and longevity of perfluorochemical-perfused hearts. *American Journal of Physiology-Heart and Circulatory Physiology.* **254** (6), H1105–H1112 (1988).
58. Sutherland, F.J., Hearse, D.J. The isolated blood and perfusion fluid perfused heart. *Pharmacological Research.* **41** (6), 613–627 (2000).
59. Werner, J.C., Whitman, V., Fripp, R.R., Schuler, H.G., Morgan, H.E. Carbohydrate metabolism in isolated, working newborn pig heart. *American Journal of Physiology-Endocrinology and Metabolism.* **241** (5), E364–E371 (1981).
60. Liao, R., Podesser, B.K., Lim, C.C. The continuing evolution of the Langendorff and ejecting murine heart: new advances in cardiac phenotyping. *American Journal of Physiology-Heart and Circulatory Physiology.* **303** (2), H156–H167 (2012).
61. Kates, R.E., Yee, Y.G., Hill, I. Effect of albumin on the electrophysiologic stability of isolated perfused rabbit hearts. *Journal of Cardiovascular Pharmacology.* **13** (1), 168–72 (1989).
62. Lou, Q., Li, W., Efimov, I.R. The role of dynamic instability and wavelength in arrhythmia maintenance as revealed by panoramic imaging with blebbistatin vs. 2,3-butanedione monoxime. *American Journal of Physiology-Heart and Circulatory Physiology.* **302** (1), H262-9 (2012).

63. Swift, L.M., et al. Properties of blebbistatin for cardiac optical mapping and other imaging applications. *Pflügers Archiv: European Journal of Physiology.* **464** (5), 503–512 (2012).
64. Kettlewell, S., Walker, N.L., Cobbe, S.M., Burton, F.L., Smith, G.L. The electrophysiological and mechanical effects of 2,3-butane-dione monoxime and cytochalasin-D in the Langendorff perfused rabbit heart. *Experimental Physiology.* **89** (2), 163–172 (2004).
65. Liu, Y. et al. Effects of diacetyl monoxime on the electrical properties of sheep and guinea pig ventricular muscle. *Cardiovascular Research.* **27** (11), 1991–1997 (1993).
66. Jou, C.J., Spitzer, K.W., Tristani-Firouzi, M. Blebbistatin effectively uncouples the excitation-contraction process in zebrafish embryonic heart. *Cellular Physiology and Biochemistry.* **25** (4–5), 419–24 (2010).
67. Sellin, L.C., McArdle, J.J. Multiple effects of 2,3-butanedione monoxime. *Pharmacology & Toxicology.* **74** (6), 305–13 (1994).
68. Cheng, Y., Li, L., Nikolski, V., Wallick, D.W., Efimov, I.R. Shock-induced arrhythmogenesis is enhanced by 2,3-butanedione monoxime compared with cytochalasin D. *American Journal of Physiology-Heart and Circulatory Physiology.* **286** (1), H310–H318 (2004).
69. Kolega, J. Phototoxicity and photoinactivation of blebbistatin in UV and visible light. *Biochemical and Biophysical Research Communications.* **320** (3), 1020–1025 (2004).
70. Sakamoto, T., Limouze, J., Combs, C.A., Straight, A.F., Sellers, J.R. Blebbistatin, a myosin II inhibitor, is photoinactivated by blue light. *Biochemistry.* **44** (2), 584–588 (2005).
71. Várkuti, B.H. et al. A highly soluble, non-phototoxic, non-fluorescent blebbistatin derivative. *Scientific Reports.* **6** (1) 26141 (2016).
72. Bray, M.A., Lin, S.F., Wikswo Jr, J.P. Three-dimensional surface reconstruction and fluorescent visualization of cardiac activation. *IEEE Transactions on Bio-medical Engineering.* **47** (10), 1382–1391 (2000).
73. Qu, F., Ripplinger, C.M., Nikolski, V.P., Grimm, C., Efimov, I.R. Three-dimensional panoramic imaging of cardiac arrhythmias in rabbit heart. *Journal of Biomedical Optics.* **12** (4), 44019 (2007).
74. Gloschat, C. *et al.* RHYTHM: An Open Source Imaging Toolkit for Cardiac Panoramic Optical Mapping. *Scientific Reports.* **8** (1), 2921 (2018).
75. Kay, M.W., Amison, P.M., Rogers, J.M. Three-dimensional surface reconstruction and panoramic optical mapping of large hearts. *IEEE Transactions on Bio-medical Engineering.* **51** (7), 1219–1229 (2004).